PHYSICAL REVIEW FLUIDS **2**, 062001(R) (2017)

Interface coupling and growth rate measurements in multilayer Rayleigh-Taylor instabilities

Raymond Adkins,[1] Emily M. Shelton,[1] Marie-Charlotte Renoult,[2]
Pierre Carles,[1,3,4] and Charles Rosenblatt[1,*]

[1]*Department of Physics, Case Western Reserve University, Cleveland, Ohio 44106, USA*
[2]*Laboratoire CORIA, Normandie Université, UNIROUEN, CNRS, LOMC, F-76000 Rouen, France*
[3]*Laboratoire FAST, Université Paris-Sud/CNRS, 23–25 rue Jean Rostand, Parc Club, F-91405 Orsay, France*
[4]*Université Pierre et Marie Curie–Paris 06, 4, place Jussieu, F-75005 Paris, France*

(Received 2 December 2016; published 19 June 2017; corrected 5 July 2017)

Magnetic levitation was used to measure the growth rate Σ vs wave vector k of a Rayleigh-Taylor instability in a three-layer fluid system, a crucial step in the elucidation of interface coupling in finite-layer instabilities. For a three-layer (low-high-low density) system, the unstable mode growth rate decreases as both the height h of the middle layer and k are reduced, consistent with an interface coupling $\propto e^{-kh}$. The ratios of the three-layer to the established two-layer growth rates are in good agreement with those of classic linear stability theory, which has long resisted verification in that configuration.

DOI: 10.1103/PhysRevFluids.2.062001

The Rayleigh-Taylor (RT) hydrodynamic instability occurs when a density gradient is subjected to an acceleration directed from the denser to the lighter fluid [1]. The slightest local deviation from hydrostatic balance creates large-scale buoyancy forces that destabilize the entire system, driving the denser fluid down and the lighter fluid up. The classical RT configuration involves a time-independent acceleration such as provided by gravity, but general RT instabilities can be associated with time-dependent accelerations. RT instabilities lie at the heart of myriad applications and diverse phenomena, for example, the discharge of fluids into larger bodies of water (such as rivers and bays), liquid impact and atomization [2], the explosion of supernovae [3,4], interface instabilities in granular media [5], as well as prosaic occurrences such as fresh paint dripping from a ceiling [6]. In inertial confinement fusion [7–9], a deuterium-tritium and polystyrene fuel pellet is subjected to laser irradiation. Nonuniformities in the irradiation profile and the original irregularities of the pellet's surface perturb the interface, setting up a RT-like instability that results in turbulence and a reduction in the compression yield.

An abundant theoretical and experimental literature is available concerning the initial stage of the instability, for which the Navier-Stokes equations can be linearized and deformation modes grow independently [1,10–14]. Consider the interface between a less dense fluid 1 of density ρ_1 and a denser fluid 2 of density ρ_2, both semi-infinite along the acceleration axis. If the acceleration points from the denser fluid to the less dense fluid, the system is unstable: In the inviscid, incompressible, and constant-acceleration case, interfacial perturbations of initial amplitude a_{k0} at wave vector k will grow with time t as $a_k(t) = a_{k0}\cosh(\Sigma t)$, where the growth rate $\Sigma = \sqrt{gk\,\mathrm{At} - [\gamma k^3/(\rho_1+\rho_2)]}$, At is the Atwood number defined as $\mathrm{At} \equiv (\rho_2-\rho_1)/(\rho_1+\rho_2)$, g is the acceleration, and γ is the surface tension [13]. For $0 < k < k_c$, where $k_c = [(\rho_2-\rho_1)g/\gamma]^{1/2}$, the perturbation is unstable, whereas for short wavelength perturbations ($k > k_c$) the interface is stabilized by surface tension. The dispersion relationship Σ vs k for the two-layer case of semi-infinite viscous fluids with surface tension was calculated long ago, and is described in Refs. [10,13]. Experimental measurements of Σ vs k date back to 1950 [11,12,14,15] and are in good qualitative, if not quantitative, agreement with theoretical predictions. One recurring problem in experimental observations of the RT instability

*rosenblatt@case.edu

is the lack of control over the initial conditions on the interface. Two of us (P.C. and C.R.) earlier demonstrated a method based on magnetic levitation to circumvent that problem [16].

The more general case of the RT instability in layered media has seen far less theoretical attention [17–22]. Experimentally, due to the difficulty in stabilizing initial conditions at not just one but several interfaces simultaneously, there are hardly any reports in the literature, with the notable exception of Ref. [23], which focuses, however, on the turbulent mixing in the late stages of the instability. With a finite central layer of dense fluid, adjacent interfaces interact strongly when their separation is comparable to, or smaller than, the wavelength $\lambda\,(=2\pi/k)$ of the interface perturbation, thereby modifying the dispersion relationships. Mikaelian used linear stability (LS) analysis for multilayer incompressible and inviscid fluids equations to obtain the dispersion relationships for the unstable interface modes [16–20]. Yang and Zhang solved a similar eigenvalue problem using a different approach [21], while Parhi and Nath derived sufficient criteria for instability of the approximate equations that describe a three-layer viscous system [22]. Despite the long-standing theoretical predictions about layered media, there are no extant results for the dispersion relationship in systems possessing three or more viscous fluid layers with two or more interfaces

Here, we measure growth rates for three-layer fluid systems, which heretofore had been inaccessible experimentally, and examine the resulting dispersion relationships in light of inviscid LS theory. We exploit our experimental technique of magnetic levitation of fluids in conjunction with magnetically permeable wires outside the liquid cell to control the wavelengths of the initial perturbations [16,24], and then make a comparison with the LS theory employed by Mikaelian [18,19]. Two separate three-layer fluid systems were examined, with ρ_i being the density of layer i, where $i = 1$ at the bottom, $i = 2$ in the middle, and $i = 3$ at the top layer. For one system we chose $\rho_1 = \rho_3 < \rho_2$, which we will refer to as "$\rho_1 = \rho_3$"; for the other system we chose $\rho_2 > \rho_1 > \rho_3$ (with air as the top layer), and refer to this as "$\rho_1 > \rho_3$." Building on Mikaelian's LS analysis [18,19], we find theoretically that the system exhibits four linearly independent eigenmodes for each wave vector k [25]. Two of these eigenmodes are related to the upper stable interface and are oscillatory, as $\rho_2 > \rho_3$. The other two modes are related to the lower unstable interface, such that one mode diverges exponentially and the other vanishes exponentially with increasing t (in the linear regime and for unstable wave vectors $k < k_c$). During the instability growth, the bottom layer amplifies its initial deformation, thus creating a fluid flow inside the finite-thickness middle layer. That fluid flow extends above (and below) the interface up to a distance of order $\exp(-kh)$, where h is the vertical extent of the middle layer. This fluid flow couples the two interfaces in such a way that an unstable deformation always grows on the upper (stable) interface, while an oscillatory deformation always appears on the lower (unstable) interface. In other words, the two interfaces "share" their eigenmodes with one another through the velocity field created in the finite fluid layer between them [25]. Our calculations that include all four modes show that, with our experimental parameters, the presence of superposed oscillatory modes on the lower interface does not impact the measure of the diverging exponential component. The growing unstable mode quickly overwhelms the other three modes, and therefore we can associate the measured growth rate of the lower interface with the unstable eigenvalue.

Based on these ideas, our central experimental results are as follows: (1) The growth rate of the unstable eigenmode is inhibited relative to the classical two-layer RT case of a single unstable interface that separates two semi-infinite layers. This effect becomes more apparent when thickness h of the middle layer is sufficiently small relative to the wavelength λ of the perturbation. This reduced growth rate is a manifestation of the coupling between the two interfaces: Not only does the lower RT-unstable interface deform with time, but so does the (intrinsically) stable upper interface. Compared to a classical RT configuration, the same local buoyancy imbalance must deform two interfaces instead of one, which explains why the growth rate should indeed be expected to be smaller than that of a single interface. (2) For each wavelength and for both the $\rho_1 = \rho_3$ case and the $\rho_1 > \rho_3$ case, the ratio by which the growth rate is reduced from the classical two-layer RT system is in excellent quantitative agreement with the predictions of Mikaelian [18]. (3) For the three-fluid

$\rho_1 > \rho_3$ case, the growth rate is systematically smaller than for the two-fluid $\rho_1 = \rho_3$ case, owing to the stronger surface tension at the air-fluid (upper) interface.

The experimental setup is described in detail elsewhere [24]. In brief, a row of straight magnetically permeable wires was spaced periodically and cemented to the front and back of a glass cell having inner width×depth×height dimensions 76×3.3×127 mm. Four sets of wires were used, having lengths 6.25, 7.5, 10, and 12.5 mm, which imposed precise harmonic perturbations on the interface corresponding to wavelengths $\lambda = 12.5$, 15, 20, and 25 mm. The cell was placed between the Faraday pole pieces of an electromagnet, such that the magnetic field exerted an upward force per volume on the liquid proportional to $\chi_i H \nabla H$, where H is the magnetic field and χ_i is the magnetic susceptibility of the fluid in layer i. Nearly magnetically inert hexadecane (liquid 1, $\rho_1 = 773\,\mathrm{kg\,m^{-3}}$, dynamic viscosity $\eta_1 = 3.26\times10^{-3}$ Pa s) was placed at the bottom of the cell to a height of 6 cm. Next, a highly paramagnetic mixture consisting of 58 wt % $MnCl_2$ $4H_2O$, 41 wt % H_2O, 1 wt % $C_{10}E_6$ surfactant, and a trace of rhodamine 6G fluorescent dye—this is the dense middle liquid 2 with $\rho_2 = 1398\,\mathrm{kg\,m^{-3}}$ and viscosity $\eta_2 = 6.24\times10^{-3}$ Pa s [26]—was placed on top of the less dense hexadecane layer 1 and supported by the upward magnetic force. Finally, for the $\rho_1 = \rho_3$ case, a second hexadecane layer ($\rho_3 = 773\,\mathrm{g\,m^{-3}}$) was placed on top of the denser aqueous mixture; for the $\rho_1 > \rho_3$ case, air ($\rho_3 \sim 0$) resided above the aqueous layer. We also performed measurements for the two-layer single-interface system, with the aqueous mixture sitting above hexadecane. The surface tension for the hexadecane-aqueous interface is $\gamma = 3.5\,\mathrm{mN\,m^{-1}}$ [26] and that of the air-aqueous interface is $\gamma = (31.1 \pm 0.2)\,\mathrm{mN\,m^{-1}}$ [27]. The cell was illuminated with a ~1 mm wide sheet of light from a Nd-YAG laser (532 nm), resulting in fluorescence from the rhodamine 6G dye in the middle layer. The fluids were imaged using a CCD video camera at 260 frames per second with resolution of 648×488 pixels, and the image in each video frame was parallax corrected.

At time $t = 0$ the magnet current was turned off, such that the circuitry facilitated a characteristic decay time 40 ms for the current and 20 ms for the magnetic force (which is proportional to the square of the current). For each of the four imposed perturbation wavelengths λ, the instability was video recorded three times for the two-layer case, and recorded five times for the three-layer system for each of two middle layer heights $h = 2$ and 5 mm in the $\rho_1 = \rho_3$ configuration, and for each of three heights $h = 1$, 2, and 5 mm in the $\rho_1 > \rho_3$ system. We remark that it was not possible to stabilize an $h = 1$ mm middle layer between two hexadecane ($\rho_1 = \rho_3$) layers. An example of a sequence of video images is shown in Fig. 1. Although it is beyond the scope of the work presented herein, it is interesting to note that a very thin layer of aqueous mixture (middle layer 2) always survives, even at very late times, between the upper and lower interfaces, i.e., layers 1 and 3 never merge (Fig. 1, last panel). This phenomenon depends on the nature and concentration of the surfactant, and will be explored in detail elsewhere.

As discussed above, for the three-layer system there are two interfaces—lower (L) and upper (U)—with four corresponding growth rates: two values for Σ_L and two for Σ_U. As $\rho_2 > \rho_3$ for both $\rho_1 = \rho_3$ and $\rho_1 > \rho_3$ configurations, the Σ_U eigenvalues are imaginary and the upper interface therefore is stable and its motion oscillatory [18]. However, we note that the upper interface also starts to deform exponentially, but with a much smaller prefactor, by its coupling to the lower interface, all the more so as h is small. We shall now equate the growth of the lower interface with the unstable eigenvalue and simply use the notation Σ for the unstable growth rate, where Σ is given in Ref. [18], Sec. IV A. The lower interface was located in each frame of the video using MATLAB's Canny algorithm [28], and was fitted over the central part of the curves (away from the edges of the cell) to the three-parameter $[A(t), B(t), \varphi(t)]$ function $z(t) = A(t)\sin[kx + \varphi(t)] + B(t)$, where wave vector $k = 2\pi/\lambda$ and λ is fixed by the choice of wires (see the green line in Fig. 1 for an example of a fitted curve). The offsets $B(t)$ varied slowly with time due to effects at the cell edges. The fitted phases $\varphi(t)$ were found to stabilize shortly after the onset of the instability, when the interfaces were no longer flat to within the limits of our imaging system. Figure 2 shows an example of $\log_e[A(t)/\lambda]$ vs t for one of the $h = 5$ mm videos. As the exponentially decreasing part of the cosh function is smaller than the experimental noise for $t > 0.05$ s, the growth rate Σ was obtained

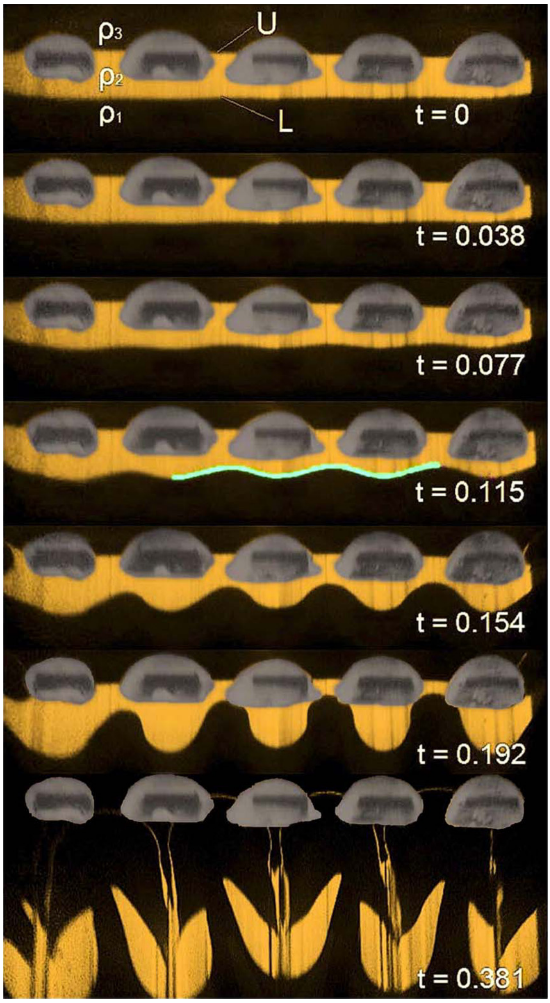

FIG. 1. A set of images vs time (in seconds) after the onset of the instability for the $h = 5$ mm, $\lambda = 12.5$ mm, $\rho_1 = \rho_3$ system. The three densities ρ_1, ρ_2, and ρ_3 are shown in the first frame, and U and L correspond to the upper and lower interfaces. The dark and gray patches visible across the U interface are the magnetically permeable wires, firmly cemented to the outside of the cell in order to create the initial L interface perturbation (they appear close to the U interface on the photograph due to parallax, but actually are located close to the L interface). A typical fitting of the lower interface is shown in the fourth frame, $t = 0.115$ s, by a green curve. The bottom frame shows the behavior at late times, where an extremely thin middle layer still separates the fluids between regions 1 and 3.

as the slope of a linear fit (in semilog scale) of an appropriate range of data in Fig. 2. To be certain that the range of fitted data was within the initial growth regime, growth rate fits were performed by first locating the earliest frame that shows a measurable instability, i.e., having an amplitude larger than a single pixel (this corresponds to time $t = 58$ ms, i.e., frame 16 in Fig. 2). We then performed a fit using the next 20 frames of the video, then 21 frames, then 22 frames, etc., until the fitted growth rates began to deviate systematically. The uncertainty in each fitted growth rate Σ was typically $\pm 0.7\ \mathrm{s}^{-1}$; it was never more than $\pm 1.0\ \mathrm{s}^{-1}$ nor less than $\pm 0.3\ \mathrm{s}^{-1}$. Figure 3 shows the experimental growth rates $\bar{\Sigma}_3$ for the three-layer system averaged over the five trials for each pair of parameters h, λ, and over three trials for the two-layer system ($\bar{\Sigma}_2$) for each value of λ. To maintain

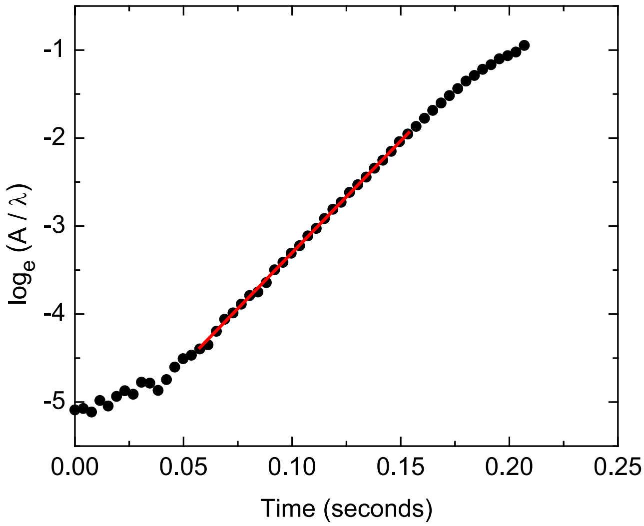

FIG. 2. The natural logarithm of the quantity fitted growth rate $A(t)$ divided by the wavelength $\lambda = 12.5$ mm obtained from each frame of the video (Fig. 1) vs time t after the magnet was turned off. Note that the seemingly nonexponential behavior at very early times is due in part to the characteristic relaxation time ($\sim$20 ms) of the magnetic force and the graininess of the image, which is exacerbated at small amplitudes.

readability of the figure, rather than plotting the error bars, we simply note that the variation of the average growth rates from the mean at each point is approximately $\pm 0.3\ \mathrm{s}^{-1}$; it was never more than $\pm 0.5\ \mathrm{s}^{-1}$ nor less than $\pm 0.2\ \mathrm{s}^{-1}$. Figure 3 clearly shows that the growth rates are reduced when the height h of the middle layer becomes small. Moreover, this reduction becomes more significant for longer wavelength perturbations, i.e., when the ratio h/λ becomes small because the coupling

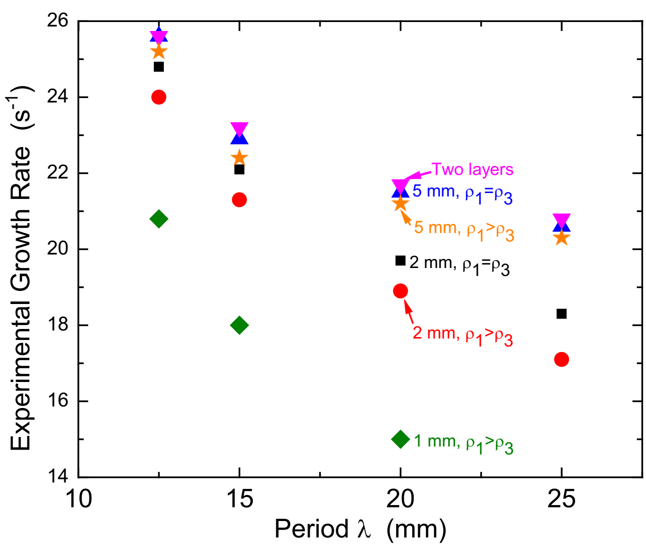

FIG. 3. The average experimental growth rates vs wavelength λ for the three-layer systems, as well as for the two-layer, single hexadecane– aqueous mixture interface system. Experimental uncertainty is discussed in the text.

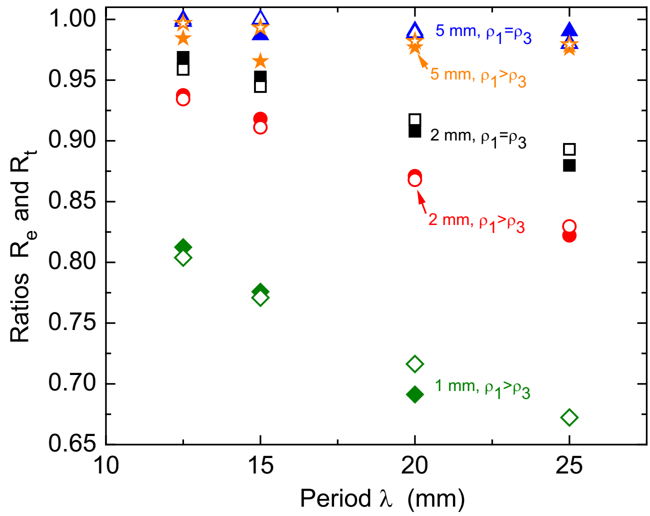

FIG. 4. The ratios R_e (experimental) and R_t (theoretical) of the unstable growth rates of the three-layer systems relative to that of the classical RT two-layer system. The solid symbols correspond to our experimental results and the open symbols to the inviscid linear stability theory calculations of Mikaelian [18]. Note that the experimental and theoretical ratios for the $h = 5$ mm, $\rho_1 = \rho_3$ case for $\lambda = 12.5$ and 20 mm nearly overlap and cannot be separated in this figure.

between interfaces becomes stronger as h decreases. We need to emphasize again that, as the entire system becomes globally unstable due to the instability of the lower interface, the upper interface also deforms exponentially—but with a smaller prefactor.

Additionally, the growth rates of the $\rho_1 > \rho_3$ system (hexadecane–aqueous mixture–air) are smaller than those of the $\rho_1 = \rho_3$ system (hexadecane–aqueous mixture–hexadecane) for a given middle layer height h and wavelength λ. This is due primarily to the much larger surface tension at the upper (aqueous mixture–air) interface, which has the effect of partially suppressing the growth of the upper interface amplitude. Due to its linear coupling with the lower interface, the growth of the lower interface is retarded accordingly.

Let us now evaluate our experimental results against theory. A *direct* comparison of growth rates from our experiment with the inviscid LS theory [18] is not appropriate because the fluids (the aqueous mixture and hexadecane) used here are viscous—about three and six times the viscosity of water, respectively—which could create especially large discrepancies when the middle layer is thin. To circumvent the limitations of the model, we chose not to compare the growth rates, but rather the *ratios* of growth rates between the two-layer and the three-layer configurations. In Fig. 4 we plot the experimental and theoretical ratios of growth rates R_e and R_t, respectively. The experimental ratios R_e are calculated as ratios of the measured growth rates in the three-layer system over those measured in the two-layer system. The theoretical ratios R_t are obtained as ratios of the growth rates predicted by LS theory for the three-layer system [18] over those predicted for the two-layer system [13]. Based on the three-layer to two-layer growth rate ratios, we find, not unexpectedly, that both R_e and R_t deviate most from unity for the smallest values of the middle layer height h and longest wavelength λ. But—and importantly—we also find for our range of parameter space (ρ,γ,h) that the experimental ratios R_e in Fig. 4 (solid symbols) appear to be in very good agreement with the theoretical ratios R_t based on Mikaelian's predictions (open symbols), with little systematic deviation between theory and experiment. This implicitly suggests that, at least in the range of parameters that we examine experimentally, the effect of viscosity couples only weakly with the finite-size effects, effectively behaving as a multiplicative factor to the growth rates. Ultimately, however, these theoretical to experimental comparisons, and the associated observation, will have to be extended to a larger parametric domain. Similarly, an in-depth analysis of the problem's equations should be conducted, in order to understand precisely why viscosity effects seem to cancel out so well in the ratios that we measured here. Nevertheless, our results suggest that the ratio of growth rates to the reference system, viz., the classical two-layer RT instability, may serve as a quantitative measure of interface coupling in the appropriate wave vector/middle layer thickness domain.

To summarize, we have experimentally explored interface coupling for a Rayleigh-Taylor instability in layered fluids. Over the range of physical parameters explored in this study, the ratio of the growth rates relative to growth rates for a single interface between two semi-infinite liquids is in very good agreement with the inviscid LS theory [13,18]. As a result of interface coupling, we observe a decrease of the growth rate when the interface separation is small relative to the wavelength of the instability.

We wish to thank Eric Nied and Stephanie Hougen for contributions to the project. This work was supported in part by the Condensed Matter Physics program of the National Science Foundation under Grant No. DMR-1505389. We thank the Partner University Fund, administered by the French Embassy in the United States, for travel support between Cleveland and Paris.

R.A. and E.M.S. contributed equally to this work.

[1] G. Taylor, The instability of liquid surfaces when accelerated in a direction perpendicular to their planes. I, Proc. R. Soc. London, Ser. A **201**, 192 (1950).

[2] D. Gueyffier and S. Zaleski, Formation de digitations lors de l'impact d'une goutte sur un film liquide, C. R. Acad. Sci. Paris, Ser. IIb **326**, 839 (1998).

[3] D. Arnett, B. Fryxell, and E. Muller, An investigation of neutrino-driven convection and the core collapse supernova mechanism using multigroup neutrino transport, Astrophys. J. Lett. **341**, L63 (1989).

[4] C. L. Fryer, A. L. Hungerford, and G. Rockefeller, Supernova explosions: Understanding mixing, Int. J. Mod. Phys. D **16**, 941 (2007).

[5] J. L. Vinningland, O. Johnsen, E. G. Flekkoy, R. Toussaint, and K. J. Maloy, Granular Rayleigh-Taylor Instability: Experiments and Simulations, Phys. Rev. Lett. **99**, 048001 (2007).

[6] M. Fermigier, L. Limat, J. E. Wesfreid, P. Boudinet, and C. Quilliet, Two-dimensional patterns in Rayleigh-Taylor instability of a thin layer, J. Fluid Mech. **236**, 349 (1992).

[7] M. H. Anderson, B. P. Puranik, J. G. Oakley, P. W. Brooks, and R. Bonazza, Shock tube investigation of hydrodynamic issues related to inertial confinement fusion, Shock Waves **10**, 377 (2000).

[8] C. Boudesocque-Dubois, S. Gauthier, and J.-M. Clarisse, Self-similar solutions of unsteady ablation flows in inertial confinement fusion, J. Fluid Mech. **603**, 151 (2008).

[9] V. Bychkov, M. Modestov, V. Akkerman, and L. E. Eriksson, The Rayleigh-Taylor instability in inertial fusion, astrophysical plasma and flames, Plasma Phys. Controlled Fusion **49**, B513 (2007).

[10] See H. J. Kull, Theory of Rayleigh-Taylor instability, Phys. Rep. **206**, 197 (1991), and references therein.

[11] D. J. Lewis, The instability of liquid surfaces when accelerated in a direction perpendicular to their planes. II, Proc. R. Soc. London, Ser. A **202**, 81 (1950).

[12] H. W. Emmons, C. T. Chang, and B. C. Watson, Taylor instability of finite surface waves, J. Fluid Mech. **7**, 177 (1960).

[13] R. Bellman and R. H. Pennington, Effects of surface tension and viscosity on Taylor instability, Q. J. Appl. Math. **12**, 151 (1954).

[14] R. L. Cole and R. S. Tankin, Experimental study of Taylor instability, Phys. Fluids **16**, 1810 (1973).

[15] J. T. Waddell, C. E. Niederhaus, and J. W. Jacobs, Experimental study of Rayleigh-Taylor instability: Low Atwood number liquid systems with single-mode initial perturbations, Phys. Fluids **13**, 1263 (2001).

[16] P. Carles, H. Huang, G. Carbone, and C. Rosenblatt, Rayleigh-Taylor Instability for Immiscible Fluids of Arbitrary Viscosities: A Magnetic Levitation Investigation and Theoretical Model, Phys. Rev. Lett. **96**, 104501 (2006).

[17] K. O. Mikaelian, Time evolution of density perturbations in accelerating stratified fluids, Phys. Rev. A **28**, 1637 (1983)

[18] K. O. Mikaelian, Rayleigh-Taylor and Richtmyer-Meshkov instabilities in multilayer fluids with surface tension, Phys. Rev. A **42**, 7211 (1990).

[19] K. O. Mikaelian, Rayleigh-Taylor instability in finite-thickness fluids with viscosity and surface tension, Phys. Rev. E **54**, 3676 (1996).

[20] K. O. Mikaelian, Rayleigh-Taylor and Richtmyer-Meshkov instabilities and mixing in stratified cylindrical shells, Phys. Fluids **17**, 094105 (2005).

[21] Y. Yang and Q. Zhang, General properties of a multilayer stratified fluids system, Phys. Fluids A **5**, 1167 (1993).

[22] S. Parhi and G. Nath, A sufficient criterion for Rayleigh-Taylor instability of incompressible viscous three-layer flow, Int. J. Eng. Sci. **29**, 1439 (1991).

[23] J. W. Jacobs and S. B. Dalziel, Rayleigh-Taylor instability in complex stratifications, J. Fluid Mech. **542**, 251 (2005).

[24] M. C. Renoult, R. G. Petschek, C. Rosenblatt, and P. Carles, Deforming static fluid interfaces with magnetic fields: Application to the Rayleigh-Taylor instability, Exp. Fluids **51**, 1073 (2011).

[25] P. Carles (unpublished).

[26] M.C. Renoult, Étude non-linéaire de l'instabilité de Rayleigh-Taylor par lévitation magnétique: du contrôle des conditions initiales au developpement de nouveaux outils d'analyse, Ph.D. thesis, UPMC Paris 06, 2012.

[27] Measured using the pendant drop technique.

[28] J. Canny, A computational approach to edge detection, IEEE Trans. Pattern Anal. Mach. Intell. **8**, 679 (1986).